Received: 14 August 2023 | Accepted: 29 January 2024

DOI: 10.1111/jpy.13451

RESEARCH ARTICLE

Temporal and spatial diversity and abundance of cryptophytes in San Diego coastal waters

Tristin Rammel | **Maitreyi Nagarkar** | **Brian Palenik**

Scripps Institution of Oceanography, University of California San Diego, La Jolla, California, USA

Correspondence
Brian Palenik, 3110 Hubbs Hall, Scripps Institution of Oceanography, University of California San Diego, La Jolla, CA 92093-0202, USA.
Email: bpalenik@ucsd.edu

Present address
Maitreyi Nagarkar, Water Research Foundation, Alexandria, Egypt

Funding information
Division of Integrative Organismal Systems, Grant/Award Number: IOS-2029299; Division of Ocean Sciences, Grant/Award Number: OCE-1637632

Editor: A.M. Wood

Abstract

Cryptophytes (class Cryptophyceae) are bi-flagellated eukaryotic protists with mixed nutritional modes and cosmopolitan distribution in aquatic environments. Despite their ubiquitous presence, their molecular diversity is understudied in coastal waters. Weekly 18S rRNA gene amplicon sequencing at the Scripps Institution of Oceanography pier (La Jolla, California) in 2016 revealed 16 unique cryptophyte amplicon sequence variants (ASVs), with two dominant "clade 4" ASVs. The diversity of cryptophytes was lower than what is often seen in other phytoplankton taxa. One ASV represented a known *Synechococcus* grazer, while the other one appeared not to have cultured representatives and an unknown potential for mixotrophy. These two dominant ASVs were negatively correlated, suggesting possible niche differentiation. The cryptophyte population in nearby San Diego Bay was surveyed in 2019 and showed the increasing dominance of a different clade 4 ASV toward the back of the bay where conditions are warmer, saltier, and shallower relative to other areas in the bay. An ASV representing a potentially chromatically acclimating cryptophyte species also suggested that San Diego Bay exerts differing ecological selection pressures than nearby coastal waters. Cryptophyte and *Synechococcus* cell abundance at the SIO Pier from 2011 to 2017 showed that cryptophytes were consistently present and had a significant correlation with *Synechococcus* abundance, but no detectable seasonality. The demonstrated mixotrophy of some cryptophytes suggests that grazing on these and perhaps other bacteria is important for their ecological success. Using several assumptions, we calculated that cryptophytes could consume up to 44% (average 6%) of the *Synechococcus* population per day. This implies that cryptophytes could significantly influence *Synechococcus* abundance.

KEYWORDS
cryptophytes, mixotrophy, *Synechococcus*

Abbreviations: HAB, harmful Algal Bloom; MRI, maximum ingestion rate; RSA, relative sequence abundance; SIO, Scripps Institution of Oceanography; SCCOOS, Southern California Coastal Ocean Observing System.

INTRODUCTION

Originally described by Christian Gottfried Ehrenberg in the early 1830s, the first appearance of cryptophytes in scientific texts defined only the genera *Chilomonas* and *Cryptomonas* without including a visual or written description of either one (Novarino, 2012). Since their first description nearly 200 years ago, a combination of complex morphological taxonomy, cryptic life history, potential cell-preservation issues, and typically moderate contribution to the total eukaryotic assemblage have limited the full characterization of cryptophyte abundance, diversity, and ecological roles (Karlusich et al., 2020; Novarino, 2012).

Cryptophytes (Cryptomonadea) have four genomes (nuclear, mitochondrial, nucleomorph, and chloroplast) due to their evolutionary origins (Douglas et al., 2001), which distinguishes them from the sister group Goniomonadea that lacks a nucleomorph (Cenci et al., 2018; Hoef-Emden et al., 2002). Molecular phylogenies are typically inferred from nuclear SSU rDNA region sequences and have revealed clusterings of certain marine and freshwater plastid-containing cryptophyte genera. Although the relationships between genera are consistent, naming conventions for these clusters (henceforth "clades") has differed across studies; here, they will be assigned as in Hoef-Emden (2008): *Chroomonas*, *Komma*, and *Hemiselmis* in clade 1; *Guillardia* and *Hanusia* in clade 2; *Cryptomonas* in clade 3; *Teleaulax*, *Geminigera*, and *Plagioselmis* in clade 4; and *Rhinomonas*, *Rhodomonas*, and *Storeatula* in clade 5 (Hoef-Emden et al., 2002; Hoef-Emden & Archibald, 2017; Marin et al., 1998; Xia et al., 2013). *Falcomonas* and *Proteomonas*, both described by only one culture, have not consistently clustered with any of these clades (Hoef-Emden, 2008; Hoef-Emden & Archibald, 2017; Xia et al., 2013). Certain environmental sequence phylogenies showed the presence of an uncultured sister taxa to the plastid-containing cryptophytes, dubbed CRY1 (Hoef-Emden & Archibald, 2017); it is still uncertain if CRY1 is heterotrophic or autotrophic or if it possesses mixed nutritional modes. Differential branching within clades has been reported (Hoef-Emden & Archibald, 2017; Johnson et al., 2016), indicating a suitably cryptic cryptophyte diversity that may necessitate further revision of intra-clade taxonomy in the future.

The factors listed above also hinder the study of cryptophyte biogeography and diversity, but it is generally acknowledged that cryptophytes are "cosmopolitan" in nature and are found in a wide range of environmental conditions (Hoef-Emden & Archibald, 2017), including polar regions (Dorrell et al., 2022). Concatenated nuclear and nucleomorph SSU rDNA region phylogenies have yielded identical matches between strains isolated from geographically distant environments (Hoef-Emden, 2008). Clade 1 is the most biogeographically widespread: All genera contain both freshwater and marine species, with even the most marine-leaning genus (*Hemiselmis*) containing at least one freshwater member (Hoef-Emden, 2008). Clades 2, 4, and 5 consist of mostly marine species, and clade 3 appears to be freshwater (Hoef-Emden, 2008). In situ ecological observations have indicated that cryptophytes (mainly from clade 4, but also from clades 1 and 5) are consistently present in coastal environments. Electron microscopic observations of cultured material from the Gulfs of Naples and Salerno taken during March of 2002–2004 showed cryptophytes comprised an average of 16.4% of the flagellate population, with *Hemiselmis* and *Plagioselmis prolonga* dominant. Cell maxima were observed in the late spring through early autumn, and the authors suggested some species seasonality was present in these environments (Cerino & Zingone, 2006). These and similar surveys may have been hindered by the difficulty inherent in microscopy-based taxonomy, with factors such as unrealized or unrecognized dimorphism (Daugbjerg et al., 2018) potentially affecting morphological identification of taxa to the species level.

DNA microarray surveys utilizing clade-specific probes in the North Sea archipelago of Helgoland from 2004 to 2006 suggested "successive pulses" of cryptophyte abundance throughout the year, with follow-up clone library studies identifying clade 4 (specifically *Teleaulax* and *Plagioselmis*) as the dominant constituents of the cryptophyte assemblage (Medlin et al., 2017; Metfies et al., 2010; Metfies & Medlin, 2004). Four flow-sorted samples from the English Channel taken during mid-late 2007 and early 2008 showed 79% of cryptophyte SSU rDNA region amplicon relative abundance explained by clade 4, with *Geminigera* and *Teleaulax* equally explaining the majority, and *Plagioselmis* the rest (37%, 35%, and 9%, respectively; Marie et al., 2010). Combined plastid 16S and nuclear 18S rRNA gene amplicon data from 1 km off Catalina Island during March and May 2014 reported that two amplicon sequence variants (ASVs) related to *Teleaulax amphioxeia* represented the single most relatively abundant eukaryotic phytoplankton ASV for 6 days during observation (Needham et al., 2018). Taken together, microscopic and molecular surveys highlight the dominance of clade 4 in marine temperate environments, with clades 1 and 5 showing a less abundant yet persistent presence.

Cryptophytes of all clades (though primarily clade 4) have been shown to be grazed by dinoflagellates of various nutritional modes (Adolf et al., 2008; Du Yoo et al., 2017; Stoecker et al., 1997). Other grazers, such as the ciliate *Mesodinium rubrum* (=*Myrionecta rubra*), engage in kleptoplasty, engulfing cryptophyte cells to retain their plastid, often for extended periods of time (Hamilton et al., 2017; Kim et al., 2017). Cryptophyte abundance may also trigger blooms of the HAB-forming species

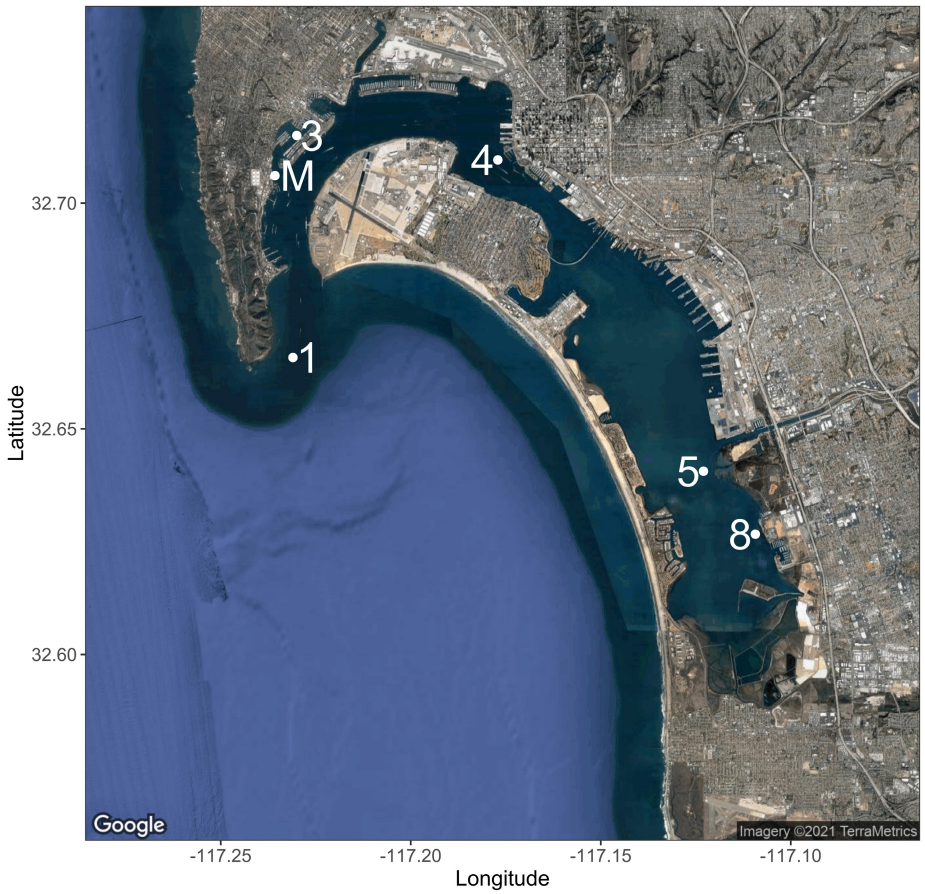

FIGURE 1 Map of sampling sites in San Diego Bay. Sites labeled numerically were collected on June 21, 2019, and site M (Marfac) was collected on July 5, 2019.

Karlodinium veneficum, which have been shown to directly graze cryptophytes (Adolf et al., 2008).

Growing evidence suggests that in addition to being prey for diverse grazers, certain cryptophytes are themselves mixotrophic on bacterial assemblages. *Cryptomonas* sp. have ingested fluorescent bacteria (Epstein & Shiaris, 1992); *Geminigera cryophila* have consumed microspheres (Gast et al., 2014); and recently, *Teleaulax amphioxeia* was proven to ingest both heterotrophic bacteria and *Synechococcus* sp. CC9311 (Du Yoo et al., 2017). Maximum ingestion rate (MIR) of *T. amphioxeia* on samples of heterotrophic bacteria was estimated to be 0.74 cells· predator^{-1}· h^{-1}, while the rate of *Synechococcus* was 0.26 cells· predator^{-1}· h^{-1} (Du Yoo et al., 2017). Cryptophytes and heterotrophic bacteria were positively correlated in Masan Bay during the former's late summer 2004 bloom season, which suggests that bacteriotrophic grazing in certain regions may contribute to cryptophyte blooms (Jeong et al., 2013).

Cryptophyte abundance and diversity is thus likely a complex result of cell loss from being grazed and cell growth from photosynthesis and mixotrophy. The goal of this paper was first to characterize the understudied molecular diversity of cryptophytes in the Southern California Bight (Scripps Institution of Oceanography Pier, a site of HAB monitoring) and nearby San Diego Bay (SD Bay; 17 miles away). San Diego Bay is connected to coastal waters but develops seasonally higher salinities and temperatures than those coastal waters (Largier et al., 1997). Second, we investigated cryptophyte abundance data in relationship to *Synechococcus* abundance as a potential prey item at the Scripps Institution of Oceanography (SIO) pier from 2011 to 2017. We also took advantage of available HAB data at the SIO pier from the Southern California Coastal Ocean Observing System (SCCOOS) program to investigate if cryptophyte abundance was related to known HAB abundance, although we had previously not seen correlations of cryptophyte ASVs and dinoflagellate ASVs using SparCC at a 0.6 cut-off level (Nagarkar & Palenik, 2023).

METHODS

Sample collection and preparation

Surface seawater was collected by bucket from the Scripps Institution of Oceanography pier in La Jolla, CA (32.8663° N, 117.2546° W) from 2011 to 2017 and

along a series of sites in SD Bay during 2019 (see Figure 1). For cryptophyte and *Synechococcus* abundance analyses at the SIO pier time series, samples were collected either weekly (before 2014) or twice per week (2014–2017). Samples from a transect of SD Bay were collected June 21, 2019, and a Site M (Marfac) bay sample was collected on July 5, 2019. Replicates of 1 mL of seawater were fixed with 10 μL of 25% glutaraldehyde (Sigma Aldrich, St. Louis, MO, USA), covered in aluminum foil to prevent light ingress, incubated at room temperature for 10 min, then stored at −80°C for flow cytometric abundance estimates.

For cryptophyte diversity analyses, samples of 500 mL of seawater were filtered in triplicate through 47 mm diameter, 0.2 μm pore size Supor filters (Pall corporation, Port Washington, NY, USA), which were wrapped in aluminum foil and stored at −80°C for extraction of environmental DNA.

Teleaulax amphioxeia (previously isolated from the SIO pier by Dr. Y. Du Yoo, strain CRYP3) and *Rhodomonas salina* CCMP 1319 were maintained in the lab, and their 18S rRNA gene sequences were analyzed. Cryptophyte stock cultures were grown in modified f/2 medium that lacked silica under continuous illumination (about 25 μmol photons $\cdot s^{-1} \cdot m^{-2}$) at 20°C, with 1 mL transferred to 20 mL new media approximately twice a month.

Collection of third-party environmental metadata

Environmental data (20 parameters) were obtained from several sources. Chlorophyll, phaeopigments, phosphate, silicate, nitrite, ammonium, nitrate, particulate domoic acid, and cell counts for *Dinophysis, Lingulodinium, Prorocentrum, Pseudo_nitzschia_delicatissima*_group, *Pseudo_nitzschia_seriata*_group, *Ceratium, Cochlodinium, and Gymnodinium* were downloaded from the ERDDAP server of SCCOOS. Details can be found at (https://erddap.sccoos.org/erddap/tabledap/HABs-ScrippsPier.html.) Daily surface temperature and salinity data for the SIO pier were provided by the Shore Stations Program sponsored at SIO by California State Parks and Recreation (https://shorestations.ucsd.edu/). Wave data including maximum height and crest-trough period were furnished by the Coastal Data Information Program, Integrative Oceanography Division, operated by the SIO.

DNA extraction

For this study, environmental DNA was extracted using two separate methods. The extraction method used on each sample is given in Table S1 in the Supporting Information. The pier samples largely used the first method as described in Nagarkar (2019). Briefly, one 0.2 μm pore size filter was removed from −80°C storage, cut into small pieces on a clean surface, placed into 2-mL tubes with 560 μL TE (50 mM tris, 20 mM EDTA), and 80 μL of 100 mg $\cdot$ mL^{-1} lysozyme. After incubation at 37°C for 30 min, 80 μL of 10% SDS and 80 μL of 10 mg $\cdot$ mL^{-1} proteinase K were added to the 2-mL tube. Following incubation for 2.5 h at 55°C, 16 μL of RNAseA were added, and the mixture was incubated for another 30 min. Two 800 μL Phenol:Choroform:Isoamyl Alcohol (P:C:IAA, 25:24:1) extractions were carried out. The resulting aqueous layer of this solution was purified using a Qiagen DNEasy Blood and Tissue kit (Qiagen, Hilden, Germany) according to the manufacturer's specifications. DNA was stored at −20°C until further use.

A second method was used on SD Bay samples, given their potentially different microbial populations that included suspended sediment microbes and higher dissolved organic carbon. For the second method, DNA was extracted using a GeneRite DNA-EZ Extraction kit (GeneRite, North Brunswick, NJ, USA) with several modifications. One 0.2 μm pore size filter was removed from −80°C storage, cut into small pieces on a clean surface, and added to an extraction tube containing preloaded 212–300 μm acid-washed glass beads (Sigma G1277). Six hundred microliters of lysis buffer (Part No. S2101) were added instead of the manufacturer-recommended 400 μL, the extraction tube was secured in a BioSpec Products Mini-Beadbeater (BioSpec Products Inc, Bartlesville, OK, USA), and the mixture was mechanically disrupted for 1 min. The tube was then centrifuged at 17,000 *g* for 1 min to pellet all glass beads at the bottom. The maximum amount of clarified supernatant (380–400 μL) was transferred into another sterile 1.7-mL microcentrifuge tube. Seven hundred and sixty microliters of binding buffer (Part No. S2201) were added to the clarified supernatant (instead of the manufacturer-recommended 600 μL) and then pipetted into a DNAsure column (Part No. S5111) that itself was placed into a collection tube (Part No. S1002). Additional steps followed the manufacturer's protocol. A total volume of 100 μL purified DNA solution was stored at −20°C until further use.

Library creation and sequencing

For SIO pier environmental samples from 2016, triplicate 25 μL PCR reactions were performed on each sample using 1 μL each of Euk1391F (5′-GTACACACCGCCCGTC-3′) and EukBr (5′-TGATCCTTCTGCAGGTTCACCTAC-3′) 18S rRNA gene primers, with single-index barcodes on the forward primer.

Additional details can be located in Nagarkar and Palenik (2023). Sequence data from 60 pier samples have been analyzed here. For cryptophyte cultures and six SD Bay samples, 20 μL of extracted and purified DNA were sent to RTL Genomics (Lubbock, Texas, USA) for sequencing on an Illumina MiSeq using the above-mentioned Euk1391 and EukBr forward and reverse primers.

Flow cytometry

Flow cytometric estimates of *Synechococcus* and cryptophyte abundance in cells · mL^{-1} were performed as in Nagarkar et al. (2021). Samples were run on a BD FACSort (Becton Dickinson, Franklin Lakes, NJ, USA) for approximately 5 min at the highest flow rate. Specific unique fluorescent populations known to contain cryptophytes or *Synechococcus* (based on runs of unialgal cultures or publications such as Marie et al., 2010) were electronically gated and enumerated by normalizing the number of events to the volume of sample run and counts of added fluorescent beads.

Amplicon sequencing data analysis

Data analysis was conducted using QIIME2 (Bolyen et al., 2019). Raw .fastq sequence data with quality scores were demultiplexed with the q2-demux plugin, then denoised with DADA2 (Callahan et al., 2016; via the q2-dada2 plugin). During this process, sequences were trimmed at 23 base pairs and truncated to 150 base pairs, as informed by the q2-demux quality score output. The results of the denoising with q2-dada2 showed that greater than or equal to 84% of the input sequences were retained as non-chimeric ASVs on all samples except for that of March 31, 2016. That sample had only 91 input sequences and retained only 19 after denoising; as such, it was removed from any and all further analyses using the feature-table filter-samples and feature-table filter-seqs commands. Amplicon sequence variants were aligned with mafft (Katoh et al., 2002) via q2-alignment, and a preliminary phylogeny was created using fasttree2 (Price et al., 2010) via the q2-phylogeny plugin. Taxonomic identity was assigned via the q2-feature-classifier plugin (Bokulich et al., 2018) using a naive Bayes classifier trained against the Silva 132 99% OTU 18S gene reference database (Quast et al., 2013) via the classify-sklearn command. Those ASVs classified as belonging to the class Cryptophyceae were exported as a biom file with relative abundance, and the sequence data were exported as a fasta-formatted text file. Several days in the time series (06/06/2016, 01/08/2016, 29/08/2016) had replicate sample extractions; these results were averaged together in the final dataset.

Phylogenetic analyses

QIIME2's Silva 132 18S rRNA gene taxonomic classifier returned 43 ASVs assigned to class Cryptophyceae. Sequences of each ASV were checked using NCBI's nucleotide Basic Local Alignment Search Tool and PR2 and using phylogenetic analysis. Nine were determined to be mis-assigned, with a few more properly members of the sister class Goniomonadophyceae (https://www.marinespecies.org/aphia.php?p=taxdetails&id=17638). These were removed for a remaining total of 34 ASVs of class Cryptophyceae. Eighteen of these sequences were determined by BLAST analysis to be nucleomorph in origin, and the remaining 16 nuclear. After compilation of the nuclear 18S rRNA gene sequences, these data and selected reference sequences from GenBank were input into the online execution of PhyML 3.0 (Guindon et al., 2010) with Smart Model Selection (Lefort et al., 2017) hosted on the ATGC bioinformatics platform (http://www.atgc-montpellier.fr/). Also included in the phylogeny were two sequences of cryptophytes in culture in the Palenik lab (*Teleaulax amphioxeia* CRYP3 and *Rhodomonas salina* CCMP 1319). Two sequences recovered from 18S rRNA gene sequencing of nearshore sampling, and one trimmed Loop Genomics long-read 18S rRNA gene sequence from August 29, 2016, all from unrelated projects, were included.

Statistical analyses in R

Particularly in the pre-2014 portion of the flow cytometric dataset, not every abundance estimate had a temporally co-occurring environmental measurement. The SCCOOS measurements were generally recorded on Monday of each week; SIO pier shore station temperature and salinity measurements were recorded daily (with some days missing data). Wave height data were recorded daily. As such, for correlation analyses between cryptophyte abundance and SCCOOS data, the data were compiled into a weekly format such that for each week from January 2011 to December 2017, there was one value for each variable. Flow cytometric data pre-2014 were only recorded on Thursdays (generally); as such, the Thursday value was used as the weekly data point. From 2014 to 2017, flow cytometry data from Mondays, directly matching SCCOOS data, were used. Temperature and salinity data were preferentially taken from the specific day of weekly cryptophyte abundance; if data were not recorded on that day, then the closest previous day with data present was used. For correlation analyses between 2016 relative sequence abundance (RSA) data and environmental variables,

12 timepoints lacked matching SCCOOS-derived measurements and were accordingly removed. For correlation analyses between cryptophyte abundance and *Synechococcus* abundance, no timepoints were removed.

Correlation analyses were performed in RStudio version 1.3.1093 with R version 4.0.3 (R Core Team, 2021). Plots were generated using a mix of Microsoft Excel and ggplot2 (Wickham, 2016), and SD Bay site maps were generated using ggmap (Kahle & Wickham, 2013). Log transformations were performed using the base R log() function. Correlation coefficients and associated *p*-values were generated using the Hmisc package (Harrell & Dupont, 2021). Shapiro tests of normality and Kolmogorov–Smirnov tests were conducted using the stats package of base R (R Core Team, 2021). Kurtosis was measured using the e1071 package (Meyer et al., 2020). All statistical tests were performed with a significance level of 0.05.

RESULTS

Flow cytometric abundance estimates 2011–2017

Flow cytometric cryptophyte abundances for 2011–2017 along with *Synechococcus* abundances are shown in Figure 2. Mean estimated cryptophyte abundance was 886 ± 1101 cells · mL^{-1} with a median of 611 cells · mL^{-1} (n = 532). Values ranged from 0 cells · mL^{-1} (no observable or distinct cryptophyte population) on October 18, 2012, to 13,118 cells · mL^{-1} on July 7, 2016. The years 2011, 2012, and 2013 were roughly equivalent in terms of median cryptophyte abundance, as were the years 2014, 2015, and 2017. The highest median abundance occurred in 2016 (885 cells · mL^{-1}), and two putative blooms in July and August reached an order of magnitude cell abundance above any other value observed in the dataset. Although the kurtosis of cryptophyte abundance distributions for all years except 2016 ranged from 0.742 to 7.18, kurtosis for the 2016 distribution was 15.775, indicating the presence of a larger right skew in the 2016 abundance relative to all other years. A two-sample Kolmogorov–Smirnov test on 2016 cryptophyte abundance (n = 101) against a distribution of all other years combined (n = 431) rejected the null hypothesis that the distribution function of all years except 2016 was greater than the distribution of 2016 abundance ($p = 1.191 \times 10^{-5}$). These two tests indicated that cryptophyte abundance during 2016 was significantly larger than other years contained in the dataset.

Maximum annual cryptophyte abundance was attained in February in 2013 and 2015, May in 2011, and between July and September in 2012, 2014, 2016, and 2017. In several cases (e.g., 2012 and 2014), the annual maximum in the late summer was preceded by a local abundance maximum of similar but slightly lower magnitude earlier in the year. Years in which the annual maxima occurred earlier in the year (e.g., 2013 and 2015) experienced a similar pattern in reverse,

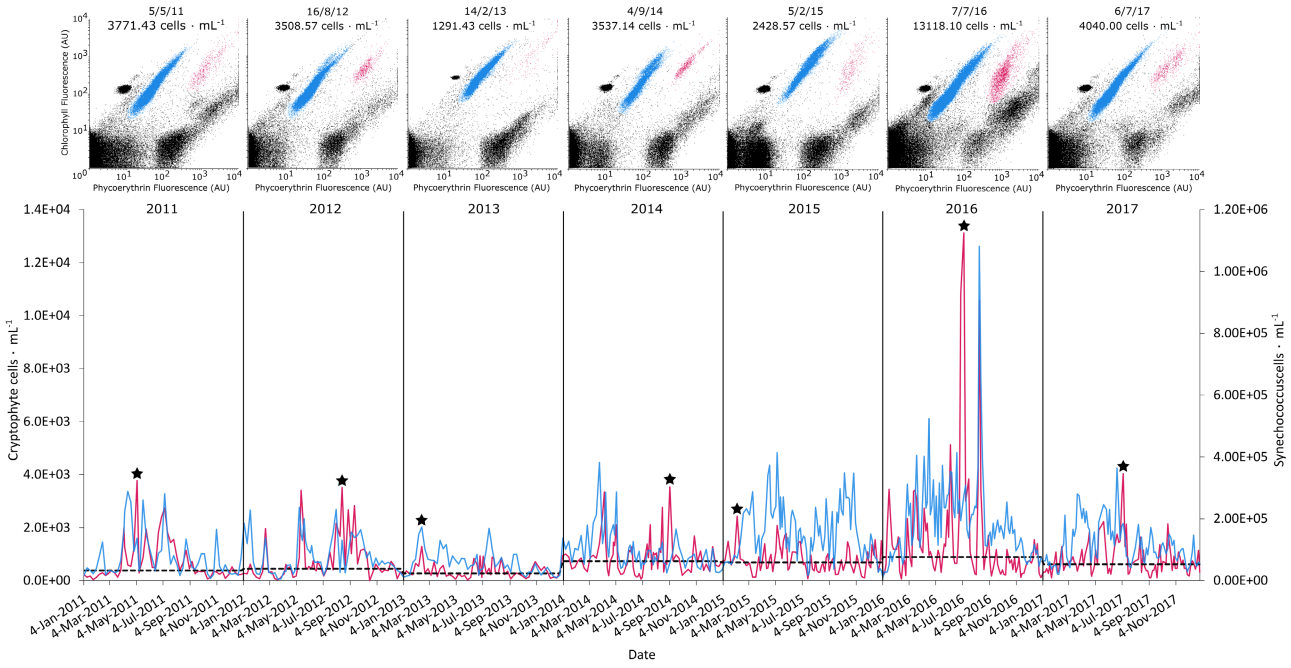

FIGURE 2 Flow cytometric cryptophyte (red) and *Synechococcus* (blue) abundance in cells · mL^{-1} off the SIO Pier from 2011 to 2017. Flow cytograms of phycoerythrin and chlorophyll fluorescence for each annual maxima (black stars) are shown above the abundance time series, with the populations measured colored correspondingly. Note the differences in scale of each *y*-axis.

presenting with a local maximum later in the year. From these data, there did not appear to be a robust seasonal pattern of cryptophyte abundance.

We examined the flow cytograms of the maximum cryptophyte abundance for each year (Figure 2) and observed variability in the distribution of flow cytometric parameters. Individual cryptophyte cell parameters were less dispersed in certain years (i.e., 2012 and 2014) with a comparatively lower variability in chlorophyll intensity for each value of phycoerythrin intensity. The interpretation of flow cytometry parameter variability is not straightforward and could represent cell physiology, actively growing versus stress cells, or mixed populations of different species with slightly different sizes and shapes present at differing ratios.

Correlation analyses of flow cytometric values with environmental variables yielded several biotic and abiotic relationships. Natural log-transformed cryptophyte and *Synechococcus* abundance estimates over the entirety of the full, non-weekly dataset ($N=532$) were the most strongly correlated with a Pearson correlation coefficient of 0.53 (p-value 0.00). When the data were fit into a weekly format (such that each flow cytometric estimate had an environmental metadata from SCCOOS or the SIO Pier shore station, see Table S2 in the Supporting Information for more information, $n=363$), cryptophytes were positively correlated with sea surface temperature ($r=0.25$, $p=2.34\times10^{-6}$), phaeopigments ($r=0.17$, $p=1.21\times10^{-3}$), silicate ($r=0.16$, $p=0.003$), and *Prorocentrum* spp. abundance ($r=0.13$, $p=0.022$), although with relatively low r values. Cryptophytes were negatively correlated with phosphate ($r=-0.13$, $p=0.014$), *Pseudo-nitzschia delicatissima* group abundance ($r=-0.13$, $p=0.013$), *Pseudo-nitzschia seratia* group abundance ($r=-0.18$, $p=0.021$), *Gymnodinium* spp. abundance ($r=-0.25$, $p=0.071$), and nitrate ($r=-0.09$, $p=0.088$). We report these, as they suggest additional avenues for research.

Phylogeny of cryptophytes in San Diego waters

Of 57 samples from the SIO Pier in 2016 containing a total of 10,585 ASVs, the Silva 132-based q2-feature-classifier script assigned 43 ASVs to class Cryptophyceae. After manual curation, nine ASVs were removed. The remaining 34 ASVs are provided in fasta format in File S1 in the Supporting Information, but all 43 ASVs can be found in Table S3 in the Supporting Information. The PR2 database queries (https://pr2-database.org) and phylogenetic analyses suggested some of the nine removed sequences were from sister groups of the Cryptophytes, but others were poorly resolved. Of the remaining 34 ASVs, 16 were determined to be cryptophyte nuclear sequences, and 18 were likely cryptophyte nucleomorphs. The ASVs from these cryptophytes represented about 2% of the total sequencing reads with a range of 0.14%–11%.

The nuclear 18S rRNA gene phylogenetic tree inferred from PhyML 3.0's GTR + G evolutionary model is shown in Figure 3. The ASVs from the pier, SD Bay, and cultures were constituents of clades 1, 4, and 5 (previously described above). The *Falcomonas daucoides* reference sequence clustered with clade 1, with longer branch lengths than representatives of *Hemiselmis*, and the *Urgorri complanatus*/*Proteomonas sulcata* references did not cluster within any clade. Representatives of the uncultured environmental CRY clade clustered within the phylogeny with long branch lengths.

Clade 4 was the most highly represented cryptophyte clade in our sequence data. Eight of 16 QIIME2-derived ASVs (ASVs 1–8), both pier nearshore sequences, and the single available Loop Genomics long-read sequence were clustered within clade 4 (*Teleaulax*, *Plagioselmis*, and *Geminigera*). Amplicon sequence variant 8 showed the shortest branch length from the node, differentiating clade 4 from the rest of the phylogeny. The closest BLAST hits to these ASVs are shown in Table S4 in the Supporting Information.

Four of 16 ASVs (ASV9, 10, 11, and 12) and the *Rhodomonas salina* CCMP 1319 culture clustered in clade 5. Reference sequences for *Rhinomonas* and *Rhodomonas* clustered with 100% identity to each other at these fragment lengths (e.g., *Rhinomonas pauca*, *nottbecki*, and *Rhodomonas* sp. CCAC 1630, data not shown). Four of 16 ASVs (ASVs 13, 14, 15, and 16) clustered with or were 100% matches to representatives of *Hemiselmis* of clade I. Details are in Table S4.

Relative sequence abundance of SIO pier cryptophytes in 2016

Fluctuations of the RSA of various ASVs relative to total cryptophyte sequences in each sample are shown in Figure 4a. Clade 4 ASVs constituted an average of 98.44% of cryptophyte RSA off the SIO pier during the study period. Amplicon sequence variant 1 (putatively *Teleaulax amphioxeia*) was the most abundant, with an average RSA of 39.66%, followed by ASV 2 (an ambiguous clade 4 sequence), with an average RSA of 33.38%. Both ASVs 1 and 2 were present on every sample date in the study period save October 17, when ASV 1's presence was not recorded. Amplicon sequence variant 3 (putatively *Plagioselmis prolonga*) had an average RSA of 13.75% and was present on all sample dates save for 2 days in September (the 19 and 26) and on October 10. For other less abundant clade 4 ASVs, see Table 1. Table S5 in the Supporting Information is a BIOM table for all 18S rRNA gene data from the SIO pier.

Clade 5 ASVs constituted an average of 1.21% of cryptophyte RSA off the SIO pier during the study period. Clade 1 ASVs constituted an average of 0.34%

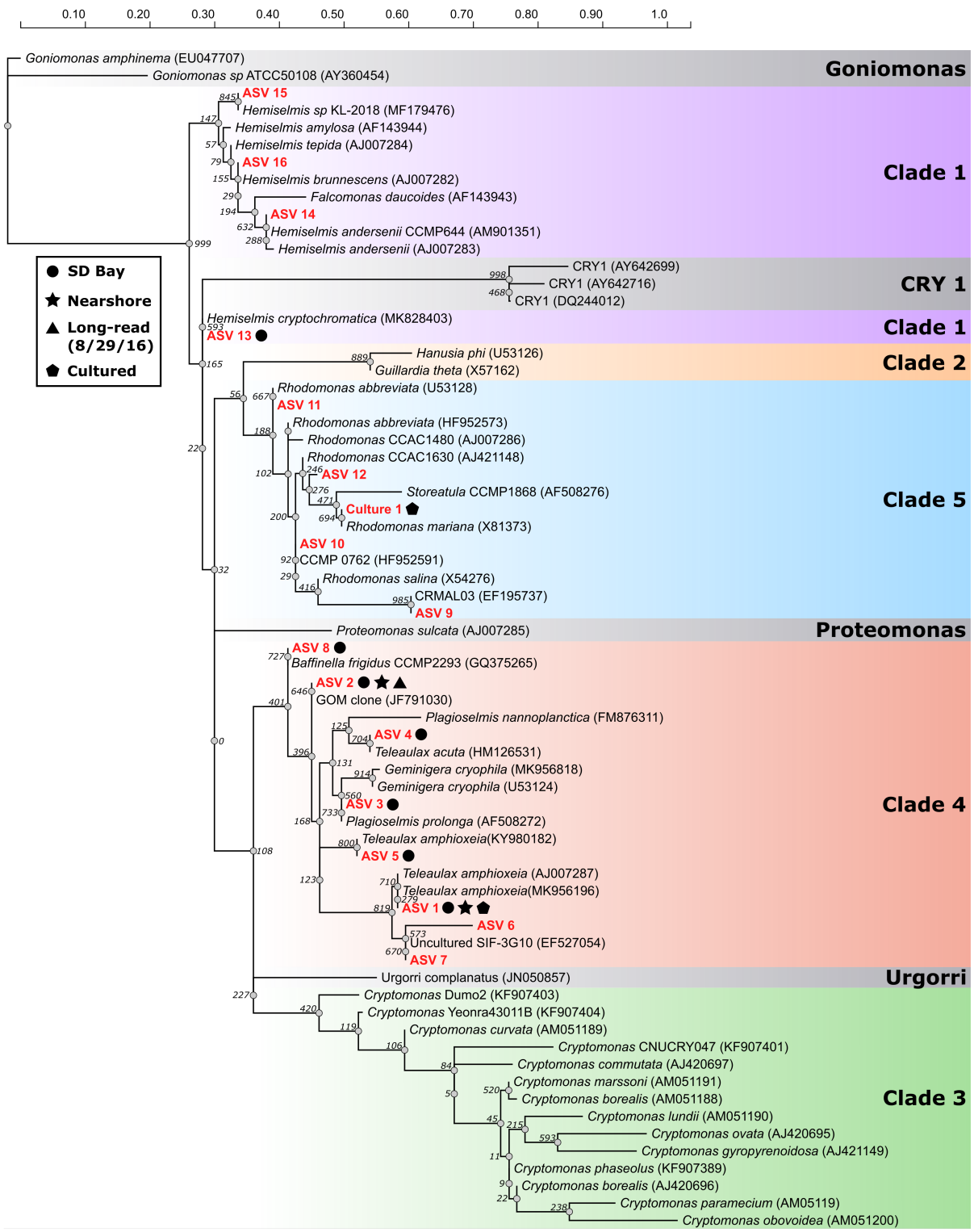

FIGURE 3 Maximum likelihood phylogenetic tree of the cryptophyte partial small subunit ribosomal 18S amplicon sequenced in this study. Bootstrap support out of 1000 replicates is placed adjacent to each node in italics. Sequences in red are ASVs recovered from the pier, bay, and cultured strains. Symbols adjacent to the sequences indicate if they were found in San Diego Bay (SD Bay) samples, nearshore samples adjacent to the SIO Pier, one long-read 18S rRNA gene sample from the SIO Pier taken August 29, 2016, or in culture.

of cryptophyte RSA off the SIO pier during the study period. Amplicon sequence variant 13 (Clade 1, putatively *Hemiselmis cryptochromatica*) had an average RSA of 0.28% and was present on less than half of the study period's sample dates, mostly present from June to August, although peak RSA occurred on March 7 (2.11%). Data on clade 1 and 5 ASVs not mentioned here can be found in Table 1.

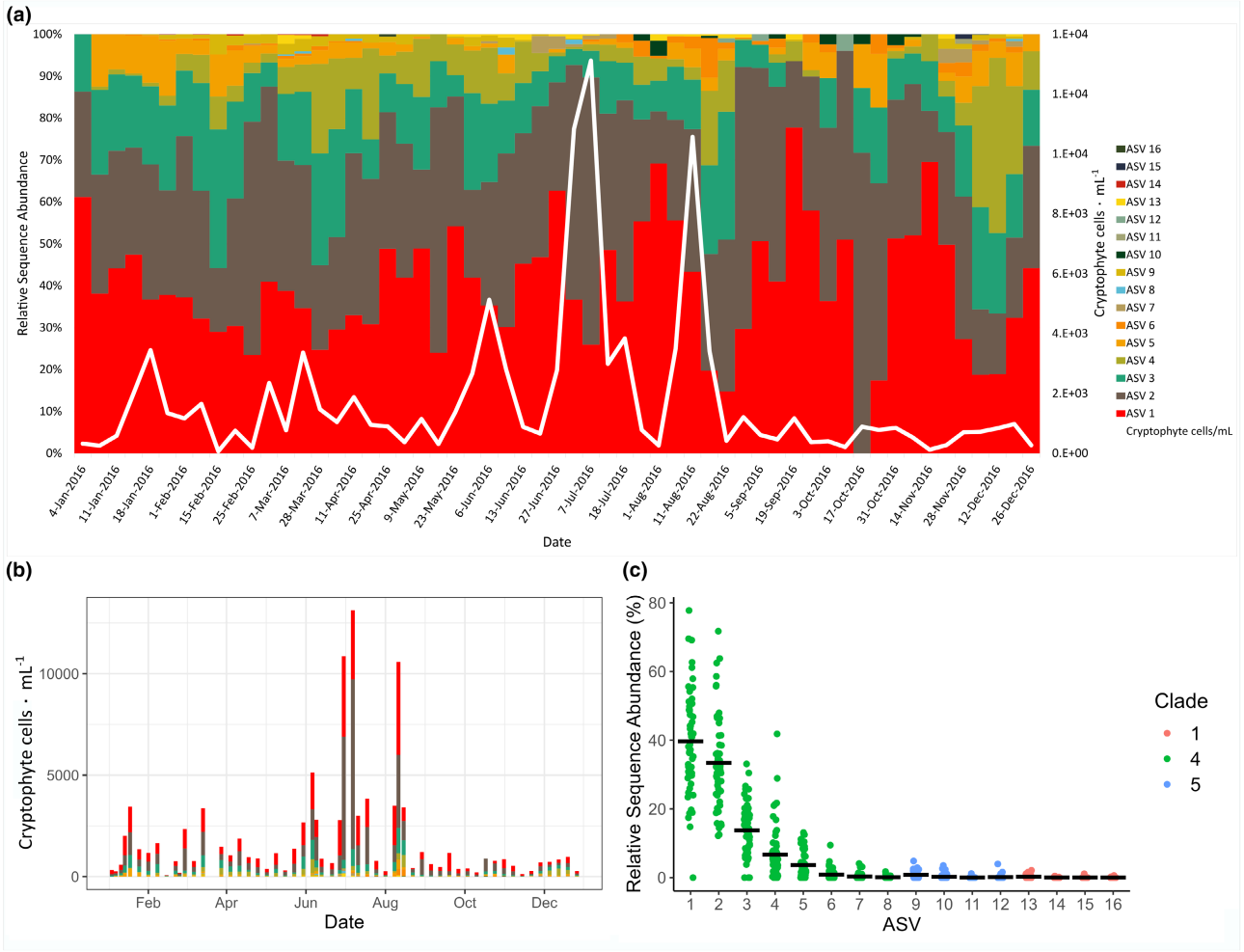

FIGURE 4 Cryptophyte ASV dynamics off the SIO Pier in 2016. (a) Stacked bar plot of cryptophyte RSA (relative sequence abundance) in 2016, overlaid with cryptophyte abundance estimates in cells · mL^{-1} (white line). (b) Flow cytometric abundance of cryptophytes at each time point subdivided by the RSA of each ASV. The ASV colors in (b) correspond to the legend of (a). (c) Jitter plot of each ASVs relative sequence abundance (RSA), with mean RSA for each ASV shown as a black line. Table S5 is a BIOM table for all 18S rRNA gene data from the SIO Pier.

In Figure 4b, we show the flow cytometric abundance of cryptophytes subdivided into ASVs using relative ASV abundance data. Although this used the assumption that species have very similar 18S rRNA gene copy numbers, it helps to demonstrate that the cryptophyte maxima ("blooms") do not appear to be blooms of single ASVs. Figure 4c shows a Jitter plot of each ASVs relative sequence abundance (RSA), with mean RSA for each ASV over all samples shown as a black line. Five Clade 4 cryptophytes clearly dominated this ecosystem, while the others appeared to be part of the "rare" biosphere.

After removing 12 RSA datapoints that lacked SCCOOS-derived data for environmental variables, interactions between natural log-transformed variables ($n = 45$) are observed. Amplicon sequence variant 1 was positively correlated with temperature, with a Pearson coefficient of 0.36 (p-value of 0.01). Amplicon sequence variant 1 was negatively correlated with ASVs 2, 3, 4, and 5 (Pearson coefficients of −0.42, −0.63, −0.39, −0.50, and with p-values of 4.20×10^{-3}, 2.96×10^{-6}, 8.34×10^{-3}, and 4.22×10^{-4}, respectively), as well as *Pseudo-nitzschia seriatia* group cells · L^{-1} with a Pearson coefficient of −0.31 (p-value of 0.04). Amplicon sequence variant 2 was positively correlated with *Gymnodinium* cells · L^{-1}, with a Pearson coefficient of 0.41 (p-value 0.005), and negatively correlated with ASV 4, with a Pearson coefficient of −0.45 (p-value 0.002). These correlations were higher than those calculated with total cryptophyte abundance that was discussed above.

Identification of nuclear/nucleomorph pairs

Cryptophytes contain 18S rRNA-containing nucleomorphs, derived from a red algal nucleus (Douglas et al., 2001). BLAST-assigned nuclear and nucleomorph sequences were correlated with one another in order to determine if species-specific sequence pairs for pier ASVs could be identified. Results are

summarized in Table 2 for nuclear sequences displaying a significantly higher correlation coefficient with a single nucleomorph than other nucleomorphs ($n = 57$). Amplicon sequence variant 1's putative nucleomorph displayed a nearly identical average RSA over 2016, whereas ASV 2's nucleomorph had an average RSA approximately 11% higher than its nuclear average. These data showed that the ratio of cryptophyte nuclear and nucleomorph 18S SSU rRNA region copy number was often near 1, as would be expected, but could vary. Nuclear ASVs not shown in Table 2 could not have a nucleomorph sequence attributed to them by these methods.

TABLE 1 Table showing the identity, clade, average RSA (relative sequence abundance, rounded), and days present for all ASVs present off the SIO Pier in 2016.

ASV	Clade	Avg RSA (%)	Days present (out of 57)
ASV 1	4	39.66	56
ASV 2	4	33.38	57
ASV 3	4	13.75	54
ASV 4	4	6.71	51
ASV 5	4	3.62	45
ASV 6	4	0.89	33
ASV 7	4	0.34	11
ASV 8	4	0.08	6
ASV 9	5	0.82	32
ASV 10	5	0.26	8
ASV 11	5	0.02	1
ASV 12	5	0.12	4
ASV 13	1	0.28	20
ASV 14	1	0.02	6
ASV 15	1	0.02	1
ASV 16	1	0.01	2

Cryptophyte spatial diversity in San Diego Bay

Figure 5 (and Table S4) shows the RSA of various cryptophyte ASVs at sampled sites in the SD Bay, as well as flow cytometric cryptophyte abundances weighted (multiplied) by the RSA for the same sites. Site 4 showed the highest flow cytometric cryptophyte abundance estimate at 6503 cells · mL^{-1}, while Site 8 in the back of the bay had the lowest cryptophyte abundance at 577 cells · mL^{-1}. No ASVs were recovered in the bay that were not recovered from SIO Pier sequencing in 2016, but large differences in the relative abundance of ASVs at the two sites are noted. For example, ASV 8 had an average RSA of 0.08% (maximum of 1.76%) off the pier over a whole year. Moving from the mouth of the bay to the back of the bay yielded a gradual increase in ASV 8's amplicon's contribution with a peak of 40.43% at site 5. In contrast to sites sampled in the main water mass of the bay, Site 3 (located in the Shelter Island Harbor, see Figure 1) showed ASV 3 (putatively *Plagioselmis prolonga*) as the most dominant ASV with 68.46% of cryptophyte RSA. Amplicon sequence variant 1 (which was correlated with temperature at the SIO pier) displayed a higher relative abundance in the warmer back bay than ASV 2, which was not correlated significantly with temperature off the pier. Amplicon sequence variant 13 had an average RSA of 0.28% and was present in less than half of 2016 pier samples, but was consistently present in SD Bay with an average RSA of 8.23%.

DISCUSSION

This study investigated the temporal and spatial fluctuations in cryptophyte abundance and diversity at

TABLE 2 Table showing ASV, average RSA (Relative Sequence Abundance), avg nuclear/nucleomorph ratios correlation coefficients, and *p* values for each identified nuclear/nucleomorph pair off the SIO Pier in 2016.

Nuclear	Avg nuclear RSA (%)	Nucleomorph	Avg Nucleomorph RSA (%)	Avg nuclear/ nucleomorph ratio	Correlation coefficient	*p*-value
ASV 1	39.66	Nucleo 14	38.91	1.02	0.9	0
ASV 2	33.38	Nucleo 17	44.77	0.75	0.9	0
ASV 3	13.75	Nucleo 1	7.07	1.94	0.83	1.33×10^{-15}
ASV 4	6.71	Nucleo 4	0.91	7.37	0.93	0
ASV 5	3.62	Nucleo 18	4.10	0.88	0.8	6.39×10^{-14}
ASV 9	0.82	Nucleo 12	0.56	1.46	0.6	9.14×10^{-7}
ASV 10	0.26	Nucleo 13	0.12	2.17	0.6	1.03×10^{-6}
ASV 11	0.02	Nucleo 16	0.10	0.20	0.43	9.49×10^{-4}
ASV 13	0.28	Nucleo 9	0.05	5.60	0.54	1.19×10^{-5}
ASV 14	0.02	Nucleo 8	0.02	1.43	0.72	3.77×10^{-10}

Note: Nuclear and nucleomorph RSA for each ASV is calculated from the total cryptophyte nuclear and nucleomorph reads separately such that nucleomorph relative abundance does not contribute to total nuclear abundance, and vice versa. Ratios are the ratio between average nuclear/nucleomorph RSA.

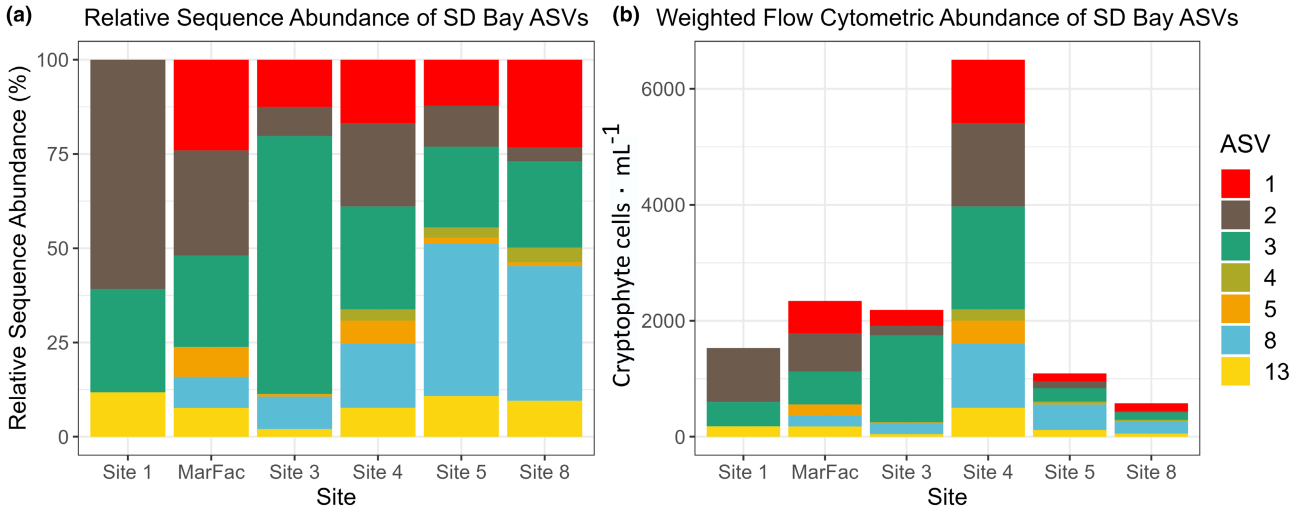

FIGURE 5 Spatial diversity of cryptophytes in San Diego Bay (SD Bay). (a) RSA (relative sequence abundance) of cryptophyte ASVs at each site in San Diego Bay shown in Figure 1. (b) Flow cytometric abundance of cryptophytes at each site subdivided by the RSA of each ASV at each site shown in Figure 1. Site M was sampled on July 5, 2019, all other sites were sampled on June 21, 2019. Tables S4 shows identity, clade, and RSA of each nuclear ASV in SD Bay. Table S6 in the Supporting Information is a BIOM table for all 18S rRNA gene data from SD BAY.

a coastal site near San Diego as well as within SD Bay. San Diego Bay maintains an open connection to coastal waters but develops seasonally higher salinities and temperatures than coastal waters and thus represents a potentially novel environmental niche for cryptophytes. Cryptophytes were consistently present in flow cytometric samples from the SIO pier from 2011 to 2017 and exhibited statistically significant positive correlations with the *Synechococcus* assemblage and sea surface temperature, as well as calculated negative correlations with phosphate and *Pseudo-nitzschia*. Cryptophytes were also consistently present in SD Bay, with maximum abundance in the mid-bay.

High-throughput amplicon sequencing found 16 nuclear 18S rRNA ASVs displaying an overwhelming dominance of clade 4 cryptophytes, particularly ASV 1 (likely *Teleaulax amphioxeia*) and ASV 2 (an unknown species). In SD Bay, there was a decrease in the dominant SIO pier ASVs' abundance and an increase in ASV 8 moving from the mouth to the back bay. Amplicon sequence variants 3 and 13 were also present in the Bay at higher abundances relative to 2016 SIO pier levels. Although the SIO Pier was analyzed in 2016 and SD Bay in 2019, the robust year-long dataset from 2016 and the strong contrast with 2019 suggests that these results represent a strong divergence in the relative abundance of species (measured as ASVs) in the two populations.

Long-term cryptophyte temporal dynamics

This study provides a valuable survey of direct cryptophyte cell abundance, showing a population off the SIO Pier from 2011 to 2017 that fluctuated in abundance throughout the year without a clearly defined seasonal bloom. Cryptophyte abundance at this research site over multi-year timescales (1997–2000) had previously been elucidated using marker photopigments (Goericke, 2011) and also showed low seasonal variation and the lack of a distinct bloom season.

Our results contrast with certain other coastal regions that have been studied. Cerino and Zingone (2006) reported cryptophyte blooms between May and September 2002–2003 from <100 cells · mL^{-1} to between 200 and 700 cells · mL^{-1} in the Gulfs of Naples and Salerno in coastal Italy. Jeong et al. (2013) recorded 26 cryptophyte-dominated blooms in Masan Bay, Korea at various magnitudes with a maximum of 392,440 cells · mL^{-1} between June and December of 2004, with no other blooms noted between June 2004 and May 2005. Kang et al. (2013) recorded three cryptophyte blooms in Shiwha Bay, Korea, from 2010 to 2012, all between March and June. In cases where species identity was recorded, "*Chroomonas (Rhodomonas) amphioxiae*" (likely a pre-taxonomic revision *Teleaulax amphioxeia*) bloomed to around 270 cells · mL^{-1} in April–July of 1969 in the Cape Fear River estuary, North Carolina, and cryptophytes in general were noted to be abundant during spring and fall in estuaries in the area (Mallin, 1994). *Plagioselmis prolonga* bloomed between 10^2 and 10^3 cells · mL^{-1} in June 2010 to a maximum of 40%–49% of the Krka River (Croatia) estuary's total phytoplankton, based on light microscopic enumeration (Supraha et al., 2014). These results highlight vast differences in the magnitude of cryptophyte blooms in different regions, including those of our study. Annual maxima off the SIO Pier suggested a "normal" maxima around 10^4 cells · mL^{-1}, although as 2016 showed, there is a potential for higher magnitudes. More research is needed to determine why different coastal regions seem to display

cryptophyte abundance seasonality (i.e., Cerino & Zingone, 2006; Kang et al., 2013) while others do not. *Synechococcus* also does not display strong seasonality at the SIO Pier (Nagarkar et al., 2018; Nagarkar et al., 2021; this study) in contrast to other sites such as Cape Cod, USA (Mackey et al., 2017) or Chesapeake Bay, USA (Wang et al., 2011). Temperature variability at these sites is much larger relative to the SIO Pier, which experiences relatively mild winters. The lack of comparatively large seasonal temperature changes at the SIO Pier may contribute to decreased seasonality of *Synechococcus* and cryptophytes.

Temperature was the strongest abiotic predictor of cryptophyte abundance, as has been observed in other temporal surveys (Jeong et al., 2013) and culture-dependent studies (Fiorendino et al., 2020). The negative correlation between cryptophytes and phosphate has also been previously described (Altenburger et al., 2020). Low absolute magnitude correlations between cryptophytes and abiotic factors such as nitrate or phosphorus may be an indicator that cryptophyte growth was not significantly limited by such nutrients or that cryptophytes may be able to use organic phosphorus, which might be relatively more abundant when inorganic phosphate is low. However, we note that the concessions necessary to fit the environmental and flow cytometric data together into a weekly format may influence the analyses, and thus the observed patterns regarding abiotic influences on cryptophyte abundance.

Cryptophyte mixotrophy

It is also possible that biotic factors may be equally or more influential than abiotic factors on abundance fluctuations off the SIO Pier. Recent research has described *Teleaulax amphioxeia* as mixotrophic on *Synechococcus* sp. (Du Yoo et al., 2017). *Synechococcus* abundance and cryptophytes showed a positive correlation from 2011 to 2017, and as our study's amplicon sequencing in 2016 showed, ASV 1 (putatively *T. amphioxeia*) was on average the most abundant cryptophyte based at least on relative sequence abundance. It may be reasonable to assume that mixotrophy regularly contributes to the fluctuation of this cryptophyte's abundance.

Du Yoo et al. (2017) calculated a maximum ingestion rate (MIR) of 6.2 *Synechococcus* prey cells · predator^{-1} · day^{-1} for cells grown phototrophically in high f/2 nutrients. Assuming most cryptophytes are mixtrophic (clade 4 was the most abundant group at the pier), and assuming that cryptophytes consumed *Synechococcus* continuously over a day, we used our cell abundance data to calculate that cryptophytes could consume 0%–44% (average 6%) of the *Synechococcus* population per day. This implies that cryptophytes could contribute significantly to drawdowns in *Synechococcus* blooms such as the one observed during the second cryptophyte cell abundance maxima in 2016. However, other grazers of *Synechococcus* are, of course, also present at coastal environments such as the SIO pier (Nagarkar et al., 2018; Yoo & Palenik, 2021).

It would be possible to make a more sophisticated estimate of cryptophyte impact on *Synechococcus* using an ingestion rate versus prey abundance curve, but more estimates of cryptophyte grazing would be needed at different temperatures and with different preconditioning regimes of light, nitrogen, phosphorus, and vitamin or iron limitation that may affect (increase) MIR. The impact of bacteria community composition on cryptophyte predation is also unclear, as predation may not be limited to *Synechococcus*. It should also be noted that protist cells of similar size have shown higher *Synechococcus* MIR (Yoo & Palenik, 2021) and faster cryptophyte grazing rates have been observed (Epstein & Shiaris, 1992).

Cryptophyte diversity and microdiversity

The presence of multiple amplicon sequence variants clustering with *Teleaulax amphioxeia* has been reported in other studies (Needham et al., 2018; Medlin et al., 2017), though in this study, only ASV 1 contributed significantly to the total assemblage. More research is needed to determine whether these lower abundance ASVs are indicative of uncharacterized microdiversity in *T. amphioxeia* or misreads during the high-throughput sequencing process, though the latter were thought to be removed by our analysis pipeline. It should also be remembered that identical sequences in this short region do not imply identical strains, genomes, or physiologies. Multiple lines of evidence point to ASV 2's identity as an unclassified clade 4 constituent that accounts for a significant amount of the relative abundance in the 2016 dataset. Neither ASV 2 nor its long-read analog had identical matches to either formally characterized species or unclassified strains in culture collection centers, and the long-read sequence did not cluster with any clade 4 reference sequence (data not shown). Although the taxonomic coverage of cryptophyte references in the Silva 132 database used to train the QIIME2 classifier is somewhat low, results from classification suggest that ASV 2 is a representative of *Geminigera*. *Geminigera* is a currently monospecific genus comprised of the cryophilic *G. cryophila*; if ASV 2 is indeed a member of *Geminigera*, then it would represent a novel species based on its sequence differences from *G. cryophila* as shown in Figure 3. Additionally, *G. cryophila*'s cryophilic character would theoretically not be conducive to high growth and abundance at the temperate thermal conditions observed at this study site. Other studies have reported the presence of *Geminigera* sp. in temperate environments

with similar abundances to those reported in this study (Marie et al., 2010), and an ASV collected from the Gulf of Mexico in 2010 (Rocke et al., 2013) matched ASV 2 with 100% similarity. Johnson et al. (2016) reported the presence of a cryptophyte partial plastid LSU RuBisCO (*rbc*L) gene sequence from a California Current sample collected off the coast of Monterey in 2013, which matched with 100% similarity to *Geminigera cryophila* CCMP 2564. These results would suggest that a significant fraction of cryptophyte RSA could be attributed to an ASV of undescribed taxonomy, perhaps a mesophilic constituent of the currently monospecific *Geminigera*. Isolating, culturing, and characterizing this cryptophyte would both help resolve the taxonomy of the class and further describe the main constituents of coastal phytoplankton assemblages in temperate environments.

One interesting finding of this study was a frequent correlation between pairs of Silva-annotated cryptophyte ASVs, but on further investigation, it was determined that one was derived from a nuclear and one from a nucleomorph 18S rRNA gene sequence. For example, ASV 1 was correlated with an ASV later designated Nucleo14 (See Table 2 for other pairs). Although this is not surprising given cryptophyte biology and the ability of general 18S rRNA gene primers to amplify both nuclear and nucleomorph genes, it does help validate our statistical analyses. One remaining puzzle is why the ratio of nuclear to putative nucleomorph reads was not always 1.0 but was occasionally as high as 2–7. One explanation is that nuclear 18S rRNA genes could be duplicated relative to the nucleomorph (or vice versa), perhaps in a cell size-dependent manner. If true, this ratio could be used as an indicator of cryptophyte cell size in field samples. It is also possible that, for a few species, the nuclear or nucleomorph 18S rRNA gene is less efficiently amplified by the primers used (primer bias) resulting in ratios different from 1. The potential use of this approach as a metric for cryptophyte size would need further validation.

SIO Pier cryptophyte dynamics in 2016

This study reinforces previous findings of clade 4 dominance in temperate marine environments (Medlin et al., 2017; Marie et al., 2010; Needham et al., 2018; Mallin, 1994; Supraha et al., 2014; and others). *Teleaulax*, *Geminigera*, and *Plagioselmis* have been identified as the dominant taxa in similar relative abundances in other temperate regions (Marie et al., 2010), but this study provids temporal resolution to the approximate species level. Although the average abundances tell a similar story to previous publications, we determined that ASV 1 was negatively correlated with ASVs 2–5, all of which experienced periods in which they comprised ~10% of cryptophyte relative abundance. These patterns are suggestive of active competition within clade 4 among members of *Teleaulax*, *Plagioselmis*, etc., or niche differentiation driven by factors such as temperature or grazing (considering cryptophytes as both predators and prey).

Increases in temperature have been identified in the increased growth rate of *Teleaulax amphioxeia* in culture studies (Fiorendino et al., 2020), and in this study, ASV 1 had the strongest positive response to increases in temperature at the SIO Pier relative to all other ASVs that contributed significantly to the cryptophyte assemblage. In addition, ASV 1 was more abundant in the warmer back bay than ASV 2. High temperature events may give *T. amphioxeia* a competitive advantage off the SIO Pier over other abundant taxa, while lower temperatures may favor ASV 2. Whatever the initiating factor for increases in ASV 1 abundance over short timescales, declines in that abundance usually followed within several weeks. *Teleaulax amphioxeia* is prey for various dinoflagellate genera of mixed nutritional modes including *Gymnodinium*, *Alexandrium*, and *Prorocentrum*, as well as the mixotrophic ciliate *Mesodinium rubrum* (=*Myrionecta rubra*), certain of which engage in kleptoplasty (figure 6 of Du Yoo et al., 2017; Stoecker et al., 1997; Adolf et al., 2008). The negative relationship seen between *Gymnodinium* and ASV 1 combined with the positive relationship between the former and ASV 2 suggests that grazers of *T. amphioxeia* may be responding to increases in ASV 1, allowing for increases in abundance of other dominant clade 4 taxa. The increase in ASVs 3 and 4 after the August 11th bloom may also be evidence of grazing on the cryptophyte assemblage that had proliferated before the dominant taxa rebound around the beginning of September. Some *Mesodinium* spp. (a ciliate grazer on cryptophytes; Moeller et al., 2021) appeared to be present based on 18S rRNA gene sequences.

Cryptophyte abundance and spatial diversity in San Diego Bay

This study highlighted significant differences in cryptophyte abundance over small spatial scales in the SD Bay. Although it is difficult to directly compare site M's abundance as it was collected July 5, 2019, for Sites 1, 3, 4, 5, and 8 (collected June 21, 2019), the highest cryptophyte abundance observed was recorded at Site 4, at the narrowest section of the bay near a bend in the bay. It is possible that the tidal forces acting on the bay's water mass cyclically concentrated cells in this narrow area or provided a different nutrient regime, leading to higher observed cryptophyte cell counts. Site 3 (located within Shelter Island Harbor, the opening of which faces the mouth of the bay) may also have acted as a "trap" for tidally influenced water masses, leading

to this site being the second most abundant population sampled on that day in our study.

Amplicon sequence variant 13 (putatively *Hemiselmis cryptochromatica*) was determined to be more relatively abundant in the bay than in all pier samples from 2016. *Hemiselmis cryptochromatica* can modulate the peak absorption wavelength of its phycobiliproteins in response to light color and quality to a higher degree than certain other cryptophytes (Heidenreich & Richardson, 2020). It is possible that the shallow depths of the bay relative to the coastal waters of the SIO pier generates a differential light profile that can benefit a species adapted to or able to acclimate to such conditions, yielding higher observed abundance in those environments, which then feeds the rest of the bay's water mass. Amplicon sequence variant 3 (*Plagioselmis prolonga*) was dominant at Site 3 (a small harbor), indicating that this ASV may be more tolerant to copper contamination from the anti-fouling paint on boat hulls or other conditions unique to that sampling site.

Amplicon sequencing at all sites described a gradual decrease in the clade 4 ASVs dominant off the pier and an increase in ASV 8, a clade 4 ASV with minimal presence off the pier, moving from the mouth of the bay to the back bay. ASV 8's nuclear 18S rRNA gene sequence clustered with 100% similarity at 96% coverage to two *Baffinella* cryptophytes in culture at Bigelow NCMA isolated from Baffin Bay: CCMP 2293 and CCMP 2045 (Daugbjerg et al., 2018). It also clustered closest to the node differentiating clade 4 from the rest of the phylogeny, as shown in Figure 3. Mitochondrial phylogenies have clustered CCMP 2293 on the same node as *Teleaulax amphioxeia* (Hu et al., 2019), and plastid phylogenies have clustered it on the same node as *T. amphioxeia*, *Rhodomonas salina*, and *Guillardia theta* (Xu et al., 2019). CCMP 2045 has been described as the species *Baffinella frigidus*, based on both molecular and morphological methods (Daugbjerg et al., 2018).

The presence of a cryptophyte ASV8, which was not abundant off the pier but was abundant in SD Bay, may be evidence for fine-scale niche partitioning within clade 4 such that some factor within the bay selects for its presence more strongly than conditions off the pier. More research is needed to isolate the cryptophyte with this ASV and describe its physiological responses relative to dominant clade 4 cryptophytes found off the pier and to its polar relatives *Baffinella*.

AUTHOR CONTRIBUTIONS

Tristin Rammel: Data curation (equal); formal analysis (lead); visualization (lead); writing – original draft (lead); writing – review and editing (equal). **Maitreyi Nagarkar:** Data curation (equal); resources (equal); writing – review and editing (supporting). **Brian Palenik:** Conceptualization (lead); formal analysis (supporting); funding acquisition (lead); writing – original draft (supporting); writing – review and editing (lead).

ACKNOWLEDGMENTS

We thank Maggie Wang for her assistance with some of the sample collection and DNA extractions; Gabrielle Meza for help with sample collection; and Ivan Moreno for help with sample analysis. We thank Brett Pickering, captain of the R/V Bob and Betty Beyster for help with sampling in SD Bay. Data were provided by the Shore Stations Program sponsored at Scripps Institution of Oceanography by California State Parks, Division of Boating and Waterways. We thank Melissa Carter, Kristi Seech, and James Fumo for their consistent help and patience with discussing and coordinating pier sampling. This research was funded by a UCSD Academic Senate Grant and NSF Grant IOS-2029299 to BP and the CCE LTER program grant OCE-1637632. Funding from the SIO Department was provided to TR.

DATA AVAILABILITY STATEMENT

Sequence data have been deposited in NCBI Genbank under Bioproject PRJNA903390, Accessions: SRR22349159-SRR22 349262. SD Bay data have been deposited as Bioproject PRJNA883423, Accessions: SAMN30994811-16.

ORCID

Brian Palenik https://orcid.org/0000-0002-3717-9046

REFERENCES

Adolf, J. E., Bachvaroff, T., & Place, A. R. (2008). Can cryptophyte abundance trigger toxic *Karlodinium veneficum* blooms in eutrophic estuaries? *Harmful Algae*, *8*(1), 119–128. https://doi.org/10.1016/j.hal.2008.08.003

Altenburger, A., Blossom, H. E., Garcia-Cuetos, L., Jakobsen, H. H., Carstensen, J., Lundholm, N., Hansen, P. J., Moestrup, O., & Haraguchi, L. (2020). Dimorphism in cryptophytes-the case of Teleaulax amphioxeia/ Plagioselmis prolonga and its ecological implications. *Science Advances*, *6*(37), eabb1611. https://doi.org/10.1126/sciadv.abb1611

Bokulich, N. A., Kaehler, B. D., Rideout, J. R., Dillon, M., Bolyen, E., Knight, R., Huttley, G. A., & Caporaso, J. G. (2018). Optimizing taxonomic classification of marker-gene amplicon sequences with QIIME 2' s q2-feature-classifier plugin. *Microbiome*, *6*, 90. https://doi.org/10.1186/s40168-018-0470-z

Bolyen, E., Rideout, J. R., Dillon, M. R., Bokulich, N., Abnet, C. C., Al-Ghalith, G. A., Alexander, H., Alm, E. J., Arumugam, M., Asnicar, F., Bai, Y., Bisanz, J. E., Bittinger, K., Brejnrod, A., Brislawn, C. J., Brown, C. T., Callahan, B. J., Caraballo-Rodriguez, A. M., Chase, J., … Caporaso, J. G. (2019). Reproducible, interactive, scalable and extensible microbiome data science using QIIME 2. *Nature Biotechnology*, *37*(8), 852–857. https://doi.org/10.1038/s41587-019-0209-9

Callahan, B. J., McMurdie, P. J., Rosen, M. J., Han, A. W., Johnson, A. J. A., & Holmes, S. P. (2016). DADA2: High-resolution sample inference from Illumina amplicon data. *Nature Methods*, *13*(7), 581. https://doi.org/10.1038/nmeth.3869

Cenci, U., Sibbald, S. J., Curtis, B. A., Kamikawa, R., Eme, L., Moog, D., Henrissat, B., Maréchal, E., Chabi, M., Djemiel, C., Roger,

A. J., Kim, E., & Archibald, J. M. (2018). Nuclear genome sequence of the plastid-lacking cryptomonad *Goniomonas avonlea* provides insights into the evolution of secondary plastids. *BMC Biology*, *16*, 137. https://doi.org/10.1186/s12915-018-0593-5

Cerino, F., & Zingone, A. (2006). A survey of cryptomonad diversity and seasonality at a coastal Mediterranean site. *European Journal of Phycology*, *41*(4), 363–378. https://doi.org/10.1080/09670260600839450

Daugbjerg, N., Norlin, A., & Lovejoy, C. (2018). *Baffinella frigidus* gen. et sp. nov. (Baffinellaceae fam. nov., Cryptophyceae) from Baffin Bay: Morphology, pigment profile, phylogeny, and growth rate response to three abiotic factors. *Journal of Phycology*, *54*, 665–680. https://doi.org/10.1111/jpy.12766

Dorrell, R. G., Kuo, A., Füssy, Z., Richardson, E. H., Salamov, A., Zarevski, N., Freyria, N. J., Ibarbalz, F. M., Jenkins, J., Karlusich, J. J. P., Steindorff, A. S., Edgar, R. E., Handley, L., Lail, K., Lipzen, A., Lombard, V., McFarlane, J., Nef, C., Vanclová, A., … Lovejoy, C. (2022). Convergent evolution and horizontal gene transfer in Arctic Ocean microalgae. *Life Science Alliance*, *6*, e202201833. https://doi.org/10.26508/lsa.202201833

Douglas, S., Zauner, S., Fraunholz, M., Beaton, M., Penny, S., Deng, L.-T., Wu, X., Reith, M., Cavalier-Smith, T., & Maier, U.-G. (2001). The highly reduced genome of an enslaved algal nucleus. *Nature*, *410*(6832), 1091–1096. https://doi.org/10.1038/35074092

Du Yoo, Y., Seong, K. A., Jeong, H. J., Yih, W., Rho, J. R., Nam, S. W., & Kim, H. S. (2017). Mixotrophy in the marine red-tide cryptophyte *Teleaulax amphioxeia* and ingestion and grazing impact of cryptophytes on natural populations of bacteria in Korean coastal waters. *Harmful Algae*, *68*, 105–117. https://doi.org/10.1016/j.hal.2017.07.012

Epstein, S. S., & Shiaris, M. P. (1992). Size-selective grazing of coastal bacterioplankton by natural assemblages of pigmented flagellates, colorless flagellates, and ciliates. *Microbial Ecology*, *23*(3), 211–225. https://doi.org/10.1007/bf00164097

Fiorendino, J. M., Smith, J. L., & Campbell, L. (2020). Growth response of *Dinophysis, Mesodinium*, and *Teleaulax* cultures to temperature, irradiance, and salinity. *Harmful Algae*, *98*, 101896. https://doi.org/10.1016/j.hal.2020.101896

Gast, R. J., McKie-Krisberg, Z. M., Fay, S. A., Rose, J. M., & Sanders, R. W. (2014). Antarctic mixotrophic protist abundances by microscopy and molecular methods. *FEMS Microbiology Ecology*, *89*(2), 388–401. https://doi.org/10.1111/1574-6941.12334

Goericke, R. (2011). The structure of marine phytoplankton communities – Patterns, rules and mechanisms. *California Cooperative Oceanic Fisheries Investigations Reports*, *52*, 182–197.

Guindon, S., Dufayard, J. F., Lefort, V., Anisimova, M., Hordijk, W., & Gascuel, O. (2010). New algorithms and methods to estimate maximum-likelihood phylogenies: Assessing the performance of PhyML 3.0. *Systematic Biology*, *59*(3), 307–321. https://doi.org/10.1093/sysbio/syq010

Hamilton, M., Hennon, G. M. M., Morales, R., Needoba, J., Peterson, T. D., Schatz, M., Swalwell, J., Armbrust, E. V., & Ribalet, F. (2017). Dynamics of *Teleaulax*-like cryptophytes during the decline of a red water bloom in the Columbia River estuary. *Journal of Plankton Research*, *39*(4), 589–599. https://doi.org/10.1093/plankt/fbx029

Harrell, F. E., & Dupont, C. (2021). Hmisc: Harrell Miscellaneous. https://cran.r-project.org/web/packages/Hmisc/index.html

Heidenreich, K. M., & Richardson, T. L. (2020). Photopigment, absorption, and growth responses of marine cryptophytes to varying spectral irradiance. *Journal of Phycology*, *56*, 507–520. https://doi.org/10.1111/jpy.12962

Hoef-Emden, K. (2008). Molecular phylogeny of phycocyanin-containing cryptophytes: Evolution of biliproteins and geographical distribution. *Journal of Phycology*, *44*(4), 985–993. https://doi.org/10.1111/j.1529-8817.2008.00530.x

Hoef-Emden, K., & Archibald, J. M. (2017). Cryptophyta (Cryptomonads). In J. M. Archibald, A. G. B. Simpson, & C. H. Slamovits (Eds.), *Handbook of the protists* (pp. 851–891). Springer International. https://doi.org/10.1007/978-3-319-28149-0_35

Hoef-Emden, K., Marin, B., & Melkonian, M. (2002). Nuclear and nucleomorph SSU rDNA phylogeny in the cryptophyta and the evolution of cryptophyte diversity. *Journal of Molecular Evolution*, *55*(2), 161–179. https://doi.org/10.1007/s00239-002-2313-5

Hu, S., Xu, Y., Xu, B., & Li, F. (2019). The complete mitochondrial genome of a marine microalgae *Cryptophyceae* sp. CCMP2293. *Mitochondrial DNA Part B Resources*, *4*(1), 848–849. https://doi.org/10.1080/23802359.2019.1568214

Jeong, H. J., Yoo, Y. D., Lee, K. H., Kim, T. H., Seong, K. A., Kang, N. S., Lee, S. Y., Kim, J. S., Kim, S., & Yih, W. H. (2013). Red tides in Masan Bay, Korea in 2004–2005: I. Daily variations in the abundance of red-tide organisms and environmental factors. *Harmful Algae*, *30*, S75–S88. https://doi.org/10.1016/j.hal.2013.10.008

Johnson, M. D., Beaudoin, D. J., Laza-Martinez, A., Dyhrman, S. T., Fensin, E., Lin, S. J., Merculief, A., Nagai, S., Pompeu, M., Setala, O., & Stoecker, D. K. (2016). The genetic diversity of *Mesodinium* and associated Cryptophytes. *Frontiers in Microbiology*, *7*, 2017. https://doi.org/10.3389/fmicb.2016.02017

Kahle, D., & Wickham, H. (2013). Ggmap: Spatial visualization with ggplot2. *R Journal*, *5*(1), 144–161.

Kang, N. S., Lee, K. H., Jeong, H. J., Yoo, D. Y., Seong, K. A., Potvin, E., Hwang, Y. J., & Yoon, E. Y. (2013). Red tides in Shiwha Bay, western Korea: A huge dike and tidal power plant established in a semi-enclosed embayment system. *Harmful Algae*, *30*, S114–S130. https://doi.org/10.1016/j.hal.2013.10.011

Karlusich, J. J. P., Ibarbalz, F. M., & Bowler, C. (2020). Phytoplankton in the Tara Ocean. *Annual Review of Marine Science*, *12*, 233–265.

Katoh, K., Misawa, K., Kuma, K., & Miyata, T. (2002). MAFFT: A novel method for rapid multiple sequence alignment based on fast Fourier transform. *Nucleic Acids Research*, *30*(14), 3059–3066. https://doi.org/10.1093/nar/gkf436

Kim, M., Drumm, K., Daugbjerg, N., & Hansen, P. J. (2017). Dynamics of sequestered Cryptophyte nuclei in *Mesodinium rubrum* during starvation and refeeding. *Frontiers in Microbiology*, *8*, 423. https://doi.org/10.3389/fmicb.2017.00423

Largier, J. L., Hollibaugh, J. T., & Smith, S. V. (1997). Seasonally hypersaline estuaries in Mediterranean-climate regions. *Estuarine, Coastal and Shelf Science*, *45*(6), 789–797. https://doi.org/10.1006/ecss.1997.0279

Lefort, V., Longueville, J. E., & Gascuel, O. (2017). SMS: Smart model selection in PhyML. *Molecular Biology and Evolution*, *34*(9), 2422–2424. https://doi.org/10.1093/molbev/msx149

Mackey, K. R. M., Hunter-Cevera, K., Britten, G. L., Murphy, L. G., Sogin, M. L., & Huber, J. A. (2017). Seasonal succession and spatial patterns of *Synechococcus* microdiversity in a salt marsh estuary revealed through 16S rRNA gene Oligotyping. *Frontiers in Microbiology*, *8*, 1496. https://doi.org/10.3389/fmicb.2017.01496

Mallin, M. A. (1994). Phytoplankton ecology of North-Carolina estuaries. *Estuaries*, *17*(3), 561–574. https://doi.org/10.2307/1352404

Marie, D., Shi, X. L., Rigaut-Jalabert, F., & Vaulot, D. (2010). Use of flow cytometric sorting to better assess the diversity of small photosynthetic eukaryotes in the English Channel. *FEMS Microbiology Ecology*, *72*(2), 165–178. https://doi.org/10.1111/j.1574-6941.2010.00842.x

Marin, B., Klingberg, M., & Melkonian, M. (1998). Phylogenetic relationships among the cryptophyta: Analyses of nuclear-encoded

SSU rRNA sequences support the monophyly of extant plastid-containing lineages. *Protist*, *149*(3), 265–276. https://doi.org/10.1016/s1434-4610(98)70033-1

Medlin, L. K., Piwosz, K., & Metfies, K. (2017). Uncovering hidden biodiversity in the Cryptophyta: New picoplanktonic clades from clone library studies at the Helgoland time series site in the southern German bight. *Vie et Milieu-Life and Environment*, *67*(1), 27–32.

Metfies, K., Gescher, C., Frickenhaus, S., Niestroy, R., Wichels, A., Gerdts, G., Knefelkamp, B., Wiltshire, K., & Medlin, L. (2010). Contribution of the class Cryptophyceae to phytoplankton structure in the German bight. *Journal of Phycology*, *46*(6), 1152–1160. https://doi.org/10.1111/j.1529-8817.2010.00902.x

Metfies, K., & Medlin, L. K. (2004). DNA microchips for phytoplankton: The fluorescent wave of the future. *Nova Hedwigia*, *79*(1–2), 321–327. https://doi.org/10.1127/0029-5035/2004/0079-0321

Meyer, D., Dimitradou, E., Hornik, K., Weingessel, A., & Leisch, F. (2020). E1071: Misc functions of the department of statistics, probability theory group (Formerly: E1071). https://CRAN.R-project.org/package=e1071

Moeller, H. V., Hsu, V., Lepori-Bui, M., Mesrop, L. Y., Chinn, C., & Johnson, M. D. (2021). Prey type constrains growth and photosynthetic capacity of the kleptoplastidic ciliate *Mesodinium chamaeleon* (Ciliophora). *Journal of Phycology*, *57*, 916–930. https://doi.org/10.1111/jpy.13131

Nagarkar, M. (2019). Temporal dynamics of marine microbial communities at the SIO pier. [Doctoral dissertation, University of California San Diego]. https://escholarship.org/uc/item/1ct9x7g8

Nagarkar, M., Countway, P. D., Du Yoo, Y., Daniels, E., Poulton, N. J., & Palenik, B. (2018). Temporal dynamics of eukaryotic microbial diversity at a coastal Pacific site. *ISME Journal*, *12*(9), 2278–2291. https://doi.org/10.1038/s41396-018-0172-3

Nagarkar, M., & Palenik, B. (2023). Diversity and putative interactions of parasitic alveolates belonging to Syndiniales at a coastal Pacific site. *Environmental Microbiology Reports*, *15*(3), 157–169. https://doi.org/10.1111/1758-2229.13138

Nagarkar, M., Wang, M., Valencia, B., & Palenik, B. (2021). Spatial and temporal variations in *Synechococcus* microdiversity in the Southern California coastal ecosystem. *Environmental Microbiology*, *23*(1), 252–266. https://doi.org/10.1111/1462-2920.15307

Needham, D. M., Fichot, E. B., Wang, E., Berdjeb, L., Cram, J. A., Fichot, C. G., & Fuhrman, J. A. (2018). Dynamics and interactions of highly resolved marine plankton via automated high-frequency sampling. *ISME Journal*, *12*(10), 2417–2432. https://doi.org/10.1038/s41396-018-0169-y

Novarino, G. (2012). Cryptomonad taxonomy in the 21st century: The first 200 years. In K. Wolowski, I. Kaczmarska, J. E. Ehrman, & A. Z. Wojtal (Eds.), *Current advances in algal taxonomy and its applications: Phylogenetic, ecological and applied perspective* (pp. 19–52). Institute of Botany, Polish Academy of Sciences.

Price, M. N., Dehal, P. S., & Arkin, A. P. (2010). FastTree 2-approximately maximum-likelihood trees for large alignments. *PLoS ONE*, *5*(3), e9490. https://doi.org/10.1371/journal.pone.0009490

Quast, C., Pruesse, E., Yilmaz, P., Gerken, J., Schweer, T., Yarza, P., Peplies, J., & Glockner, F. O. (2013). The SILVA ribosomal RNA gene database project: Improved data processing and web-based tools. *Nucleic Acids Research*, *41*(D1), D590–D596. https://doi.org/10.1093/nar/gks1219

R Core Team. (2021). R: A language and environment for statistical computing. https://www.R-project.org/

Rocke, E., Jing, H. M., & Liu, H. B. (2013). Phylogenetic composition and distribution of picoeukaryotes in the hypoxic northwestern coast of the Gulf of Mexico. *Microbiology*, *2*(1), 130–143. https://doi.org/10.1002/mbo3.57

Stoecker, D. K., Li, A. S., Coats, D. W., Gustafson, D. E., & Nannen, M. K. (1997). Mixotrophy in the dinoflagellate *Prorocentrum minimum*. *Marine Ecology Progress Series*, *152*(1–3), 1–12. https://doi.org/10.3354/meps152001

Supraha, L., Bosak, S., Ljubesic, Z., Mihanovic, H., Olujic, G., Mikac, I., & Vilicic, D. (2014). Cryptophyte bloom in a Mediterranean estuary: High abundance of *Plagioselmis* cf. *prolonga* in the Krka River estuary (eastern Adriatic Sea). *Scientia Marina*, *78*(3), 329–338. https://doi.org/10.3989/scimar.03998.28C

Wang, K., Wommack, K. E., & Chen, F. (2011). Abundance and distribution of *Synechococcus* spp. and Cyanophages in the Chesapeake Bay. *Applied and Environmental Microbiology*, *77*(21), 7459–7468. https://doi.org/10.1128/aem.00267-11

Wickham, H. (2016). *ggplot2: Elegant graphics for data analysis*. Springer-Verlag.

Xia, S., Liu, G. X., & Hu, Z. Y. (2013). Morphological examination and phylogenetic position of two newly recorded freshwater *Cryptomonas* species (Cryptophyceae) from China. *Journal of Systematics and Evolution*, *51*(2), 212–222. https://doi.org/10.1111/j.1759-6831.2012.00227.x

Xu, K., Hu, S., & Tang, X. (2019). The complete plastid genome of a marine microalgae *Cryptophyceae* sp. CCMP2293 (Cryptophyta). *Mitochondrial DNA Part B Resources*, *4*(2), 2159–2160. https://doi.org/10.1080/23802359.2019.1623725

Yoo, Y. D., & Palenik, B. (2021). Growth and grazing of the chlorarachniophyte *Bigelowiella natans* (Chlorarachniophyceae) on the marine cyanobacterium *Synechococcus*. *Phycologia*, *60*(4), 375–383. https://doi.org/10.1080/00318884.2021.1941567

SUPPORTING INFORMATION

Additional supporting information can be found online in the Supporting Information section at the end of this article.

File S1. Fasta file sequences of all Amplicon Sequence Variants recovered from the SIO pier and San Diego Bay sites.

Table S1. Sample metadata including date and location of collection, type of sample taken, method of processing, and other pertinent information.

Table S2. Organizational scheme of weekly flow cytometric and environmental timeseries from 2011 to 2017.

Table S3. Table of QIIME2 Feature ID, ASV ID as assigned in this work, sequence, QIIME2-assigned taxonomy, taxonomic confidence, and sequence reads for all cryptophytes observed on sampling dates in 2016 off the SIO Pier.

Table S4. Table of additional taxonomic information on cryptophyte ASVs. Part of the table shows identity, clade, and RSA (Relative Sequence Abundance) of each ASV at each of the sampled San Diego Bay sites shown in Figure 1. Site M was sampled on 05/07/2019, all other sides were sampled on 21/06/2019.

Table S5. Table of QIIME2 Feature ID, ASV ID as assigned in this work, sequence, QIIME2-assigned taxonomy, taxonomic confidence, and sequence

reads for all 18S rRNA gene sequences recovered on sampling dates in 2016 off the SIO Pier.

Table S6. Table of QIIME2 Feature ID, ASV ID as assigned in this work, sequence, QIIME2-assigned taxonomy, taxonomic confidence, and sequence reads for all 18S rRNA gene sequences recovered on sampling dates for San Diego Bay.

How to cite this article: Rammel, T., Nagarkar, M., & Palenik, B. (2024). Temporal and spatial diversity and abundance of cryptophytes in San Diego coastal waters. *Journal of Phycology*, *00*, 1–17. https://doi.org/10.1111/jpy.13451